

# 1 Slowdown of Shirase Glacier, East Antarctica, caused by strengthening alongshore winds

2

3 Bertie W.J. Miles\*<sup>1,2</sup>, Chris R. Stokes<sup>2</sup>, Adrian Jenkins<sup>3</sup>, Jim .R. Jordan<sup>3,4</sup>, Stewart .S.R. Jamieson<sup>2</sup>,  
4 G. Hilmar. Gudmundsson<sup>3</sup>

5

6 <sup>1</sup>School of Geosciences, Edinburgh University, Edinburgh, EH8 9XP, UK

7 <sup>2</sup>Department of Geography, Durham University, Durham, DH1 3LE, UK

8 <sup>3</sup>Department of Geography and Environmental Sciences, Northumbria University, Newcastle upon  
9 Tyne, NE1 8ST, UK

10 <sup>4</sup>Laboratoire de Glaciologie, Université Libre de Bruxelles, Brussels, Belgium

11 \*Correspondence to [Bertie.Miles@ed.ac.uk](mailto:Bertie.Miles@ed.ac.uk)

12

## 13 Abstract

14 Around large parts of West Antarctica and in Wilkes Land, East Antarctica, increased wind-forced  
15 intrusions of modified Circumpolar Deep Water (mCDW) onto the continental shelf have been  
16 associated with mass loss over the last few decades. **Despite considerable seasonal variability,**  
17 **observations in 2018** ~~Observations~~ have also confirmed relatively high basal melt rates of up to 16 m  
18 a<sup>-1</sup> underneath the Shirase ice tongue in Enderby Land, East Antarctica. These high basal melt rates  
19 are also caused by intrusions of mCDW onto the continental shelf, but the catchment of Shirase  
20 Glacier has been gaining mass, a trend often attributed to increased precipitation. Here, we document  
21 the dynamical ocean-driven slowdown, ice surface thickening and grounding line advance of Shirase  
22 Glacier, in response to strengthening easterly winds that reduce mCDW inflow and decrease basal  
23 melt rates. Our findings are significant because they demonstrate that warm ice shelf cavity regimes  
24 are not universally associated with glacier acceleration and mass loss in Antarctica, and they highlight  
25 the overlooked role of the impact of easterly winds in the recent mass gain of the Shirase Glacier  
26 catchment.

27

## 28 1. Introduction

29 Shirase Glacier is one of the fastest flowing outlet glaciers in East Antarctica, reaching speeds in  
30 excess of  $2,200 \text{ m a}^{-1}$  across its grounding line, before flowing into Lützow-Holm Bay (Fig. 1). Its  
31 annual ice discharge approaches  $15 \text{ Gt a}^{-1}$  (Rignot et al., 2019) and it drains a catchment containing  
32  $1.2 \text{ m}$  of sea level equivalent (Fig.1, Morlighem et al., 2020). This rapid ice flow speed is associated  
33 with vigorous melt underneath its floating tongue, where basal melt rates were observed to vary over  
34 the course of the year between  $7$  and  $16 \text{ m a}^{-1}$  in 2018,  $16 \text{ km}$  downstream of the glacier's grounding  
35 line (Hirano et al., 2020). These high melt rates are caused by warm modified Circumpolar Deep  
36 Water (mCDW) intruding onto the continental shelf and being transported directly to the glacier via  
37 bathymetric troughs (Fig. 1; Moriwaki & Yoshida, 1983; Hirano et al., 2020), a process referred to  
38 as Mode 2 melting (Jacobs et al., 1992). Elsewhere in Antarctica, most regions that experience this  
39 mode of oceanic melt have been losing mass e.g. the Amundsen Sea (Jenkins et al., 2018; Mouginit  
40 et al., 2014), the Western Antarctic Peninsula (Cook et al., 2016) and Wilkes Land (Rintoul et al.,  
41 2016; Greene et al., 2017; Stokes et al., 2022); and hinting that intrusions of mCDW have become  
42 more potent over recent decades in these locations. However, mass loss has not been observed in the  
43 Shirase Glacier catchment and, between 2003 and 2019, its drainage basin (sometimes referred to as  
44 drainage basin 7 in Antarctic-wide studies (e.g. Smith et al., 2020) gained mass at a rate of  $+25 \pm 6$   
45  $\text{Gt a}^{-1}$ , which is the largest magnitude of imbalance of all drainage basins in East Antarctica (Smith  
46 et al., 2020), including the comparatively well studied drainage basin 13 in Wilkes Land ( $-20 \pm 14 \text{ Gt}$   
47  $\text{a}^{-1}$ ).

48 The mass gain and thickening in the Shirase catchment over the past two decades (Schröder et al.,  
49 2019; Smith et al., 2020) has been hypothesized to have been caused by increased precipitation across  
50 the wider Dronning Maud and Enderby Land regions (Smith et al., 2020). Prior to this, however,  
51 earlier field-based estimates, using repeat triangulation surveys in 1969 and 1973, demonstrated ice  
52 surface lowering of around  $0.7 \text{ m a}^{-1}$  around  $100\text{-}200 \text{ km}$  inland of the Shirase Glacier grounding line  
53 (Mae & Naruse, 1978; Naruse, 1979; Nishio et al., 1989). Furthermore, repeat GPS surveys in 1980  
54 and 1988 revealed a thinning rate of around  $0.5 \text{ m a}^{-1}$  around  $100\text{-}150 \text{ km}$  inland of the grounding  
55 line (Toh et al., 1992). These rates of surface lowering during that time are comparable with some of  
56 the fastest rates of thinning observed across Antarctica over the past decade and occurred at similar  
57 distances inland of the grounding line (Smith et al., 2020). Moreover, this surface lowering in the  
58 1970s and 1980s may have been part of a much longer-term signal with ice core records estimating  
59 a surface lowering of  $350 \text{ m}$  over the past 2000 years of the Mizuho Plateau (Kameda et al., 1990),  
60 which is located around  $200 \text{ km}$  inland of the Shirase coastline. The surface lowering over the past  
61 2000 years is also coincident with an increase in ice discharge from the Lützow-Holm Bay, which  
62 has been estimated from subglacial erosion rates (Sproson et al., 2021).

63 Oceanographic observations in Lützow-Holm Bay in 2018 have revealed a two-layered structure with  
64 a cool and relatively fresh layer of Winter Water overlying a warm and saline layer of mCDW, where  
65 temperatures near the ice front seasonally exceed the *in situ* melting point by 2.7 °C (Hirano et al.,  
66 2020). Observations and modelling demonstrate a strong seasonal variation in the basal melt rate of  
67 the Shirase ice tongue (Hirano et al., 2020; Kusahara et al., 2021), which is caused by seasonal  
68 variations in the depth of the thermocline forced by the strength of the alongshore easterly winds near  
69 the continental shelf (Ohshima et al., 1996). To date, there is no evidence of large seasonal variations  
70 in ice flow speed at the grounding line, but observations show some seasonal variation in ice flow  
71 speed on the floating tongue that could be connected to external forcing (Nakamura et al., 2007;  
72 2010).

73 There have been several studies analysing the ice flow dynamics of the Shirase Glacier, largely  
74 covering short sub-decadal time periods (Pattyn & Derauw, 2002; Pattyn & Naruse, 2003; Nakamura  
75 et al., 2010; Aoyama et al., 2013). However, the longer-term geological signal of ice sheet thinning  
76 and increased ice discharge (Sproson et al., 2021), along with observations of thinning in the 1970s  
77 and 1980s (Mae & Naruse, 1978; Naruse, 1979; Nishio et al., 1989; Toh et al., 1992), followed by  
78 thickening from the 2000s (Schröder et al., 2019; Smith et al., 2020) raise some important questions  
79 into the processes causing this switch from mass loss to mass gain. In this study, we produce a time  
80 series of ice flow speed that spans 47 years and show that long-term ice speed trends coincide with  
81 alongshore wind speeds and their impact on intrusions of mCDW. We then discuss how these  
82 observations may relate to wider hemispheric trends in atmospheric circulation and what this may  
83 mean for the future mass balance of the Shirase catchment and the wider Dronning Maud and Enderby  
84 Land sectors.

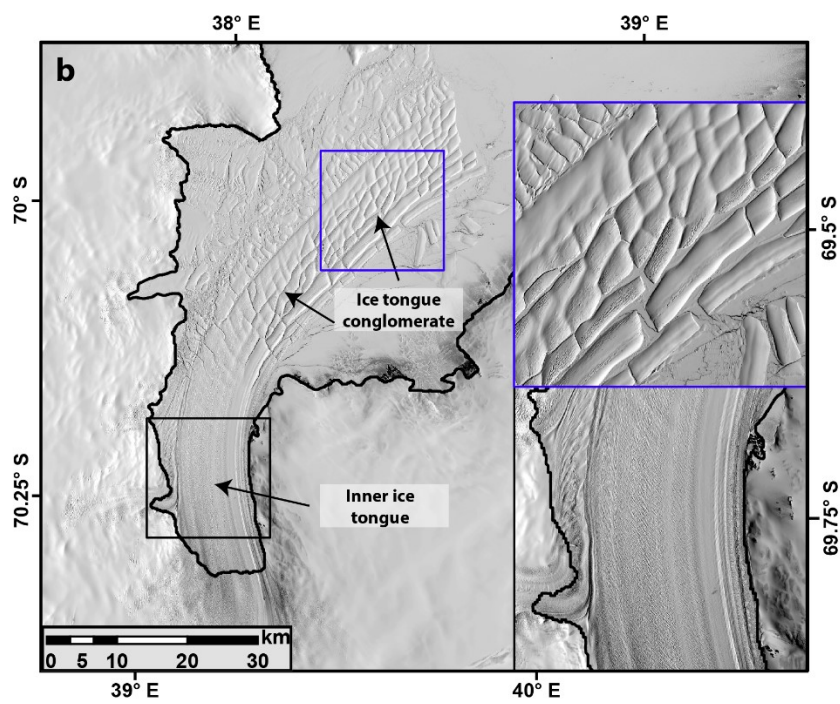
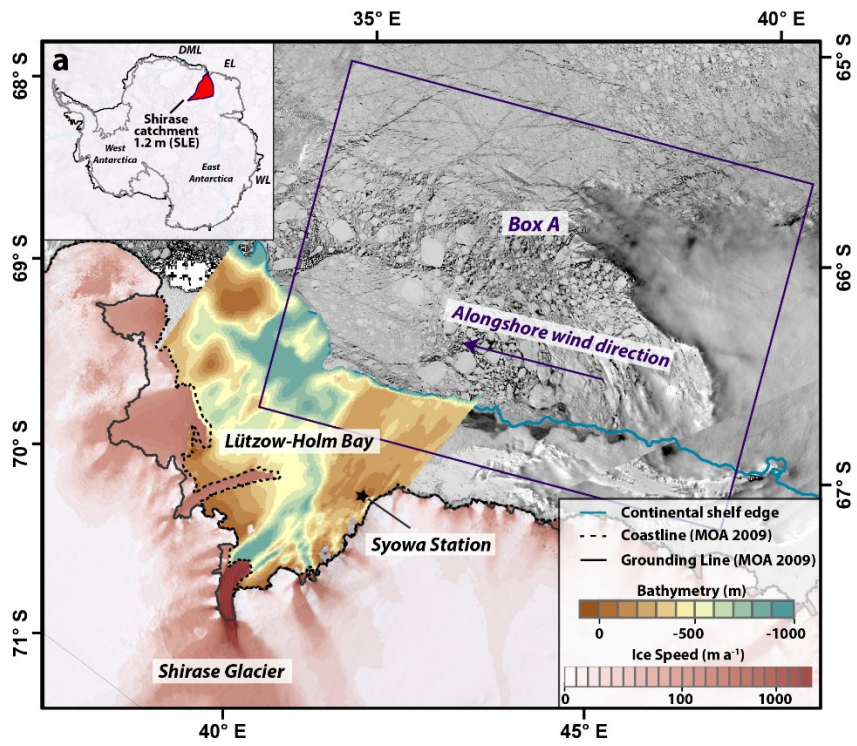
85

## 86 **2. Data and Methods**

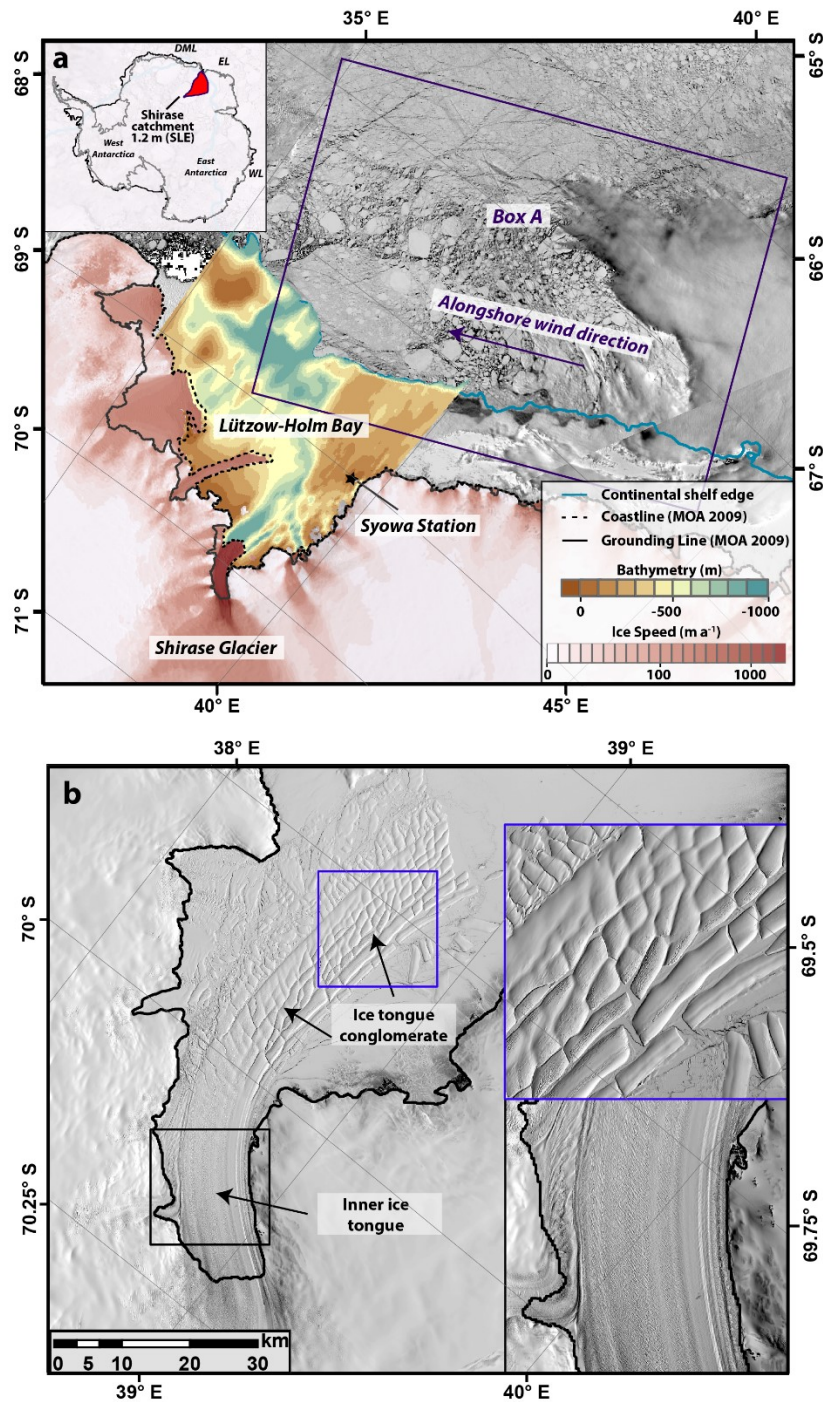
### 87 **2.1 Ice-front position, ice speed, grounding line and ice thickness**

88 We create a time series of ice-front positions between 1963 and 2020 using a variety of different  
89 sources including: ARGON imagery from 1963, Landsat-1 imagery from 1973, Landsat-5 imagery  
90 from 1984, Landsat-4 imagery from 1988, RADARSAT RAMP mosaic from 1997 (Jezek et al.,  
91 2013), and MODIS imagery from 2000-2020, with the spatial resolution of the satellite data ranging  
92 from 15-250 m. In each case, we map the outer limit of the collection of loosely bound icebergs that  
93 form the Shirase ice tongue that are typically surrounded by a smoother surface of fast ice (Fig. 1 &  
94 2a). Errors associated with this mapping are insignificant in the context of the ice tongue typically  
95 advancing 2,500 m a<sup>-1</sup>, or retreating in short-lived calving events typically greater than 10 km.

96 We calculate 18 ice speed estimates for Shirase Glacier between 1973 and 2020. For 1973 we use a  
97 pair of Landsat-1 (band 7) images from the 25<sup>th</sup> January 1973 and the 21<sup>st</sup> January 1974 that we  
98 manually co-register to each other, before co-registering to a Landsat-8 image. The combination of  
99 the relatively coarse Landsat-1 imagery (60 m) and the development of surface melt ponding over the  
100 fast-flowing section of the glaciers between the two images prevented the automatic extraction of ice  
101 speed. Instead, we extract an ice speed estimate by manually tracking the displacement of a prominent  
102 rift ~24 km downstream of the grounding line (Fig. 2ed). Errors associated with the manual tracking  
103 of this rift stem from the co-registration between the two image pairs which we estimate to be one







105

106 **Figure 1:** a) MODIS image of Lützow-Holm Bay and Shirase Glacier from the 4<sup>th</sup> November 2019  
 107 obtained from NASA WorldView. Overlain is the ITS\_LIVE composite velocity product in  
 108 logarithmic scale (Gardner et al., 2018; 2020), 1000 m bathymetric contour obtained from  
 109 BedMachine (Morlighem et al., 2020) which is taken as the continental shelf boundary and  
 110 bathymetry of the Lützow-Holm Bay (Kusahara et al., 2021). Note the deep trough connecting Shirase  
 111 Glacier to the open ocean. The location of the Syowa research station and Box A, the region where  
 112 ERA5 derived winds were extracted are also shown. The initials in the inset refer to the following,  
 113 DML (Dronning Maud Land), EL (Enderby Land), WL (Wilkes Land). b) Landsat 8 image from  
 114 November 2020 showing the structure of the Shirase ice tongue. The blue box is a zoomed in section  
 115 of the ice tongue conglomerate that is unconstrained. The black box is a zoomed in section of the  
 116 inner section of the ice tongue that is constrained by fjord walls on either side. The black line on both

117 images is the MODIS 2009 grounding line and coastline (Scambos et al., 2007; Harran et al., 2019).  
118 Landsat images are courtesy of the U.S. Geological Survey.

119

120 pixel (60 m; Animation S1). For 1988, we use a pair of Landsat-4 (band 3) images from the 14<sup>th</sup>  
121 January 1988 and the 15<sup>th</sup> February 1988 that we also co-register to a Landsat-8 image. The quality  
122 of the Landsat-5 images (30 m resolution) is superior to that of the Landsat-1 imagery and, in the  
123 absence of significant surface melt ponding, we use the feature tracking software COSI-CORR  
124 (Leprince et al., 2007; Scherler et al., 2008) to extract ice speed. For these images, co-registration  
125 error is negligible (Animation S2) and error in the feature tracking is estimated at <0.5 pixels (e.g.  
126 Heid and Kääb, 2012). Because of the close time separation of the image pairs this results in a larger  
127 error of  $\pm 171 \text{ m a}^{-1}$ .

128 For 2000-2018 we use 14 annual ice speed mosaics from the ITS\_LIVE dataset which cover Shirase  
129 Glacier (Gardner et al., 2018) and use the corresponding error grids for error values, which range  
130 from  $\pm 1$  to  $\pm 32 \text{ m a}^{-1}$ . For 2019 ( $n = 27$ ) and 2020 ( $n = 19$ ) we take an average of all GoLIVE generated  
131 ice speed fields (Fahnestock et al., 2016; Scambos et al., 2016) with a time separation of 16-320 days  
132 from scene ID's 149\_109 and 150\_109. Taking an average of multiple ice speed grids reduces error  
133 and, as such, we prescribe a nominal error of  $16 \text{ m a}^{-1}$ , based on the average value from the ITS\_LIVE  
134 mosaics. We extract ice speed profiles from each time period across a transect, T1 (Fig. 2a), and also  
135 produce a time-series of ice speed change where T1 crosses the grounding line. In 1973, the only  
136 possible observation of ice speed was extracted 24 km downstream of the grounding line (Point x;  
137 Fig. 2a) and there are no observations directly at the grounding line. To account for this, we estimate  
138 ice speed at the grounding line in 1973 using the average difference between point x, 24 km  
139 downstream of the grounding line, and where T1 crosses the grounding line in each of the other 17  
140 ice speed profiles (1988-2020). Across these profiles, ice speed was on average 2% slower (ranging  
141 from 1% to 4%) at the grounding line, compared to ice speed at point x. Therefore, to estimate ice  
142 speed at the grounding line in 1973 we reduce the ice speed observed 24 km downstream of the  
143 grounding line by  $2 \pm 1\%$ . We also include the measurements of ice speed from Nakamura et al. (2007)  
144 at the grounding line derived from the JERS-1 satellite in 1996, 1997 and 1998.

145 To estimate the direction and magnitude of any migration in the Shirase Glacier grounding line we  
146 compare time stamped digital elevation model (DEM) strips with a spatial resolution of 2 m from the  
147 6<sup>th</sup> January 2013 and the 8<sup>th</sup> October 2015 from the REMA project (Howat et al., 2019). We select  
148 these strips because they cover the complete Shirase Glacier grounding line and represent the longest  
149 time gap in the record. This is in addition to a SPOT5-HRS DEM from the SPIRIT project (Korona  
150 et al., 2009) from the 8<sup>th</sup> February 2008, with a spatial resolution of 40 m. Elevation uncertainty is

151 estimated at around 4 m by comparing derived elevations from exposed bedrock between the two  
152 REMA DEM's and a larger uncertainty of around 7 m between the SPOT5-HRS and REMA DEM's.  
153 The tidal amplitude of the region is limited to 0.2 m (Aoki et al., 2000) and is deemed insignificant.  
154 We extract elevation profiles along transect T1 (Fig. 2a) from these dates. A comparison of elevation  
155 profiles cannot provide a location of the true grounding line position, but any horizontal migration of  
156 these elevation slopes can provide reasonable estimates in both the direction and rate of grounding  
157 line migration (Fricker et al., 2009; Brunt et al., 2010).

158 We also extract an ice thickness change time-series from the dataset presented in Schröder et al.  
159 (2019) from point IT, which is around 20 km inland of the grounding line (Fig. 2a). This multi-  
160 mission dataset spans between 1978 and 2017 and contains data from a variety of satellites. We use  
161 the accompanying uncertainty estimates described in Schröder et al. (2019). We also utilize modelled  
162 basal melt rate anomalies of the Shirase ice tongue that are derived by an ocean model that is forced  
163 by ERA-Interim wind reanalysis between 2008 and 2018 by Kusahara et al. (2021). The basal melt  
164 rate dataset contains melt anomalies that have been simulated with fast ice cover and a hypothetical  
165 no fast ice scenario (see Fig. 20; Kusahara et al., 2021). We use the melt rates with fast ice cover  
166 because persistent fast ice cover remained throughout our observational period, aside from a few  
167 sporadic partial breakouts in the summer months.

168

## 169 **2.2 Climatological data**

170 We extract mean monthly ERA5 (Hersbach et al., 2020) 10 m zonal (U) and meridional winds (V)  
171 speeds with a gridded 30 km spatial resolution between 1979 and 2021 from a box approximately  
172 340 x 250 km adjacent to the coastline (Box A; Fig. 1a). We do not extend the box all the way into  
173 Lützow-Holm Bay because it is semi-permanently covered with landfast sea-ice (Fig. S1) that  
174 dampens the impact of winds on ocean circulation. We then calculate alongshore easterly wind speed  
175 using an alongshore angle of 80° from due north:

$$176 \quad A = W \cos(\theta - 80)$$

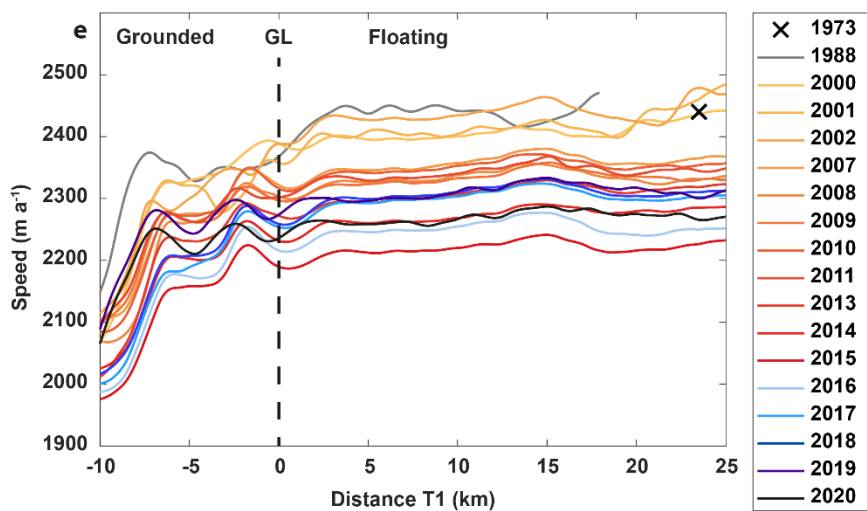
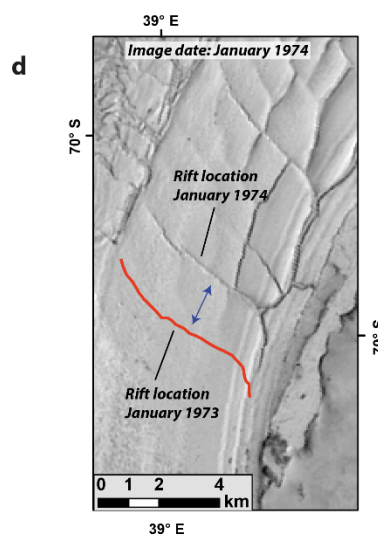
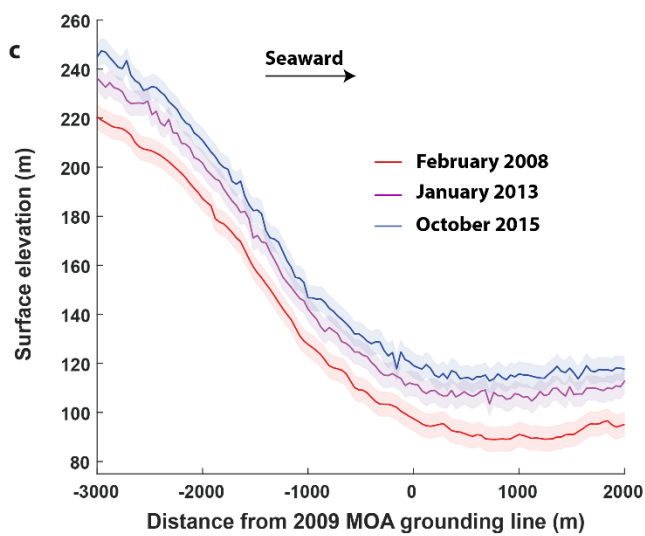
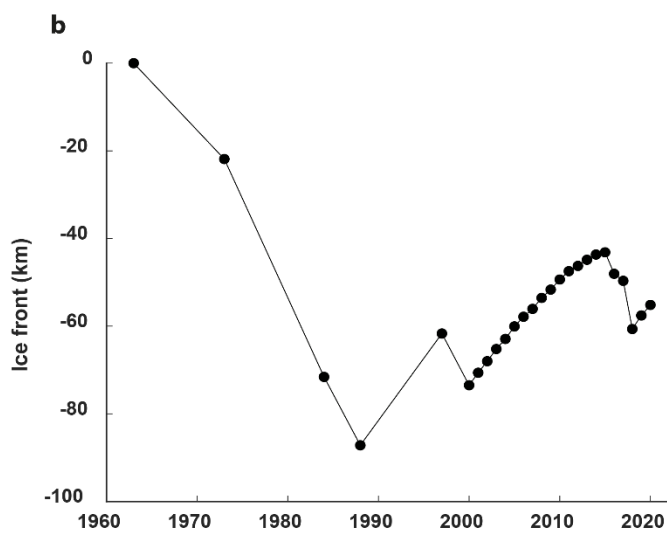
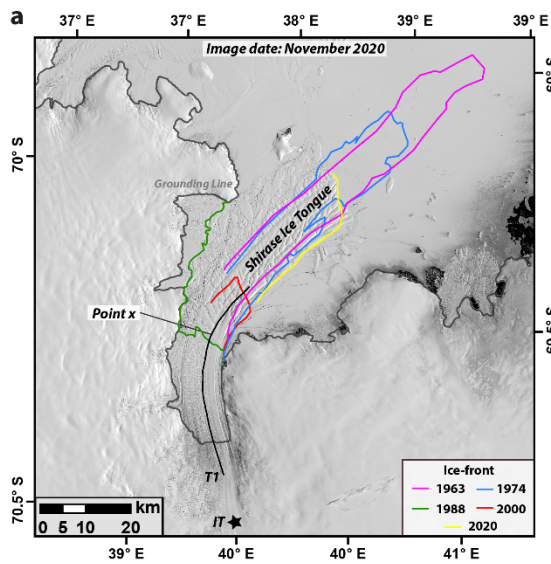
177 Where  $W$  is wind speed and  $\theta$  is wind direction. Using the ERA5 data, we also calculate the linear  
178 trend in zonal wind between 1979 and 2021 across a wider region of the Dronning Maud and Enderby  
179 Land coastlines. We also extract a precipitation time series across Shirase Glacier using the regional  
180 climate model MAR between 1979 and 2019 (Kittel et al., 2021).

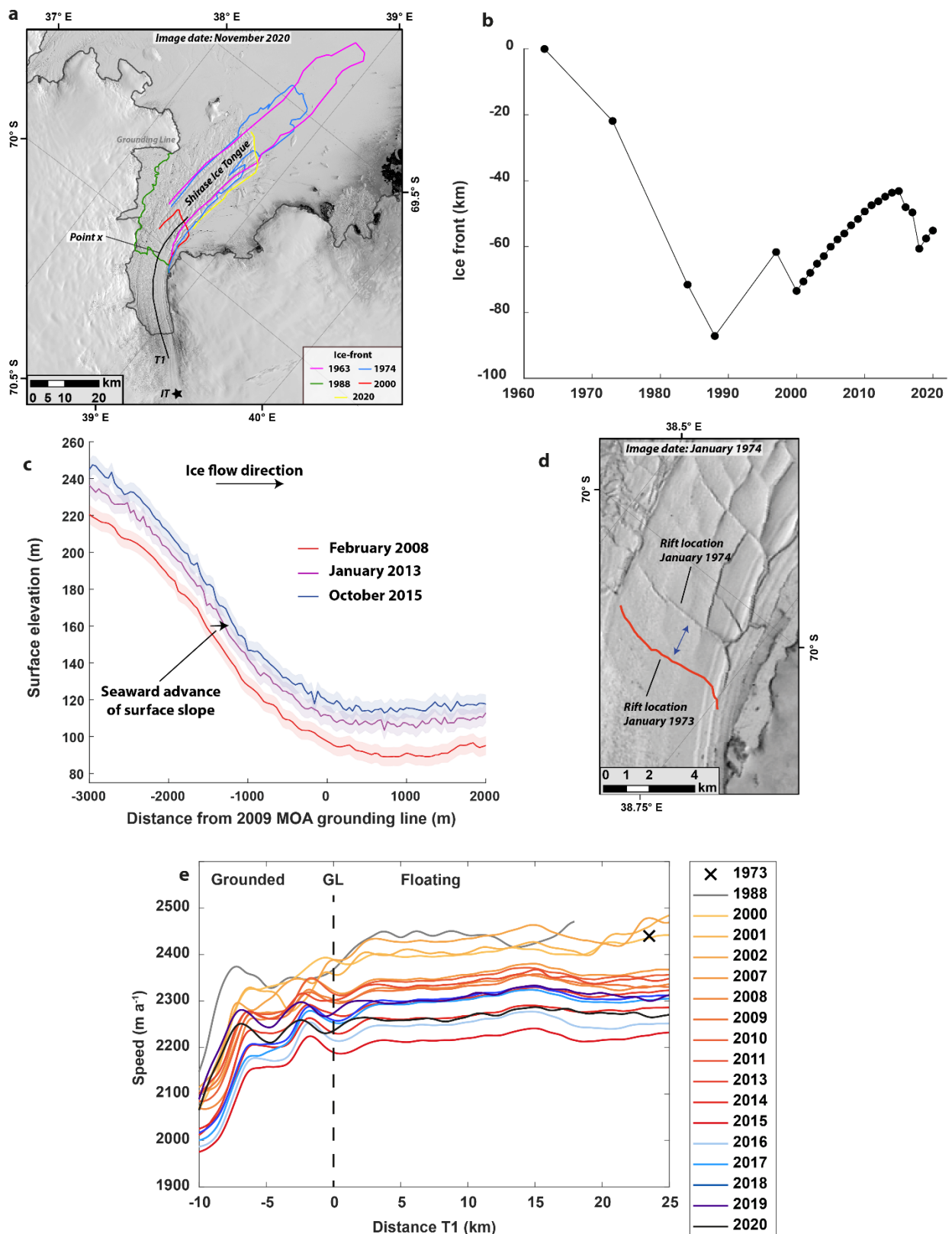
181

## 182 **3. Results**



183 We observe a total range of nearly 90 km in the ice-front position of the Shirase ice tongue between  
184 1963 and 2020 (Fig. 2a, b). Its maximum length was in 1963, before retreating to its minimum extent  
185 in 1988 (Fig. 2a, b). Since 1988 there has been a general pattern of advance with a few sporadic  
186 calving events (Fig. 2a, b). Most of the variation in the extent of the Shirase ice tongue is in the  
187 heavily fractured and unconstrained ice tongue conglomerate (Fig. 1b; Fig. 2a). The only exception  
188 to this was in 1988 when the ice tongue retreated to the entrance of the narrow and more constrained  
189 section of its fjord, 24 km advanced of its 2009 grounding line (Fig. 2a).





191

192 **Figure 2:** a) Landsat-8 image from November 2020 showing the Shirase ice tongue. Overlain are  
 193 selected ice-front positions from 1963, 1974, 1988, 2000 and 2020; along with the transect, T1, used  
 194 to extract ice speed profiles and point x, which is the location of the 1973/74 ice speed estimate on  
 195 the floating tongue. Point IT is the location of the ice thickness time-series. The grey line is the  
 196 MODIS 2009 grounding line (Scambos et al., 2007, Harran et al., 2021). b) Change in ice-front extent

197 relative to 1963. **c)** Surface elevation profiles along a small section of T1 as it intersects the grounding  
198 line from February 2008, January 2013 and October 2015 showing a seaward migration of the surface  
199 slope **d)** Landsat-1 image showing the rift used to estimate ice speed in 1973/74. The red line is the  
200 digitized rift from January 1973. **e)** Ice speed profiles from transect T1 between 1973 and 2020. The  
201 black cross represents the ice speed measurement from 1973/74. Landsat images are courtesy of the  
202 U.S. Geological Survey.

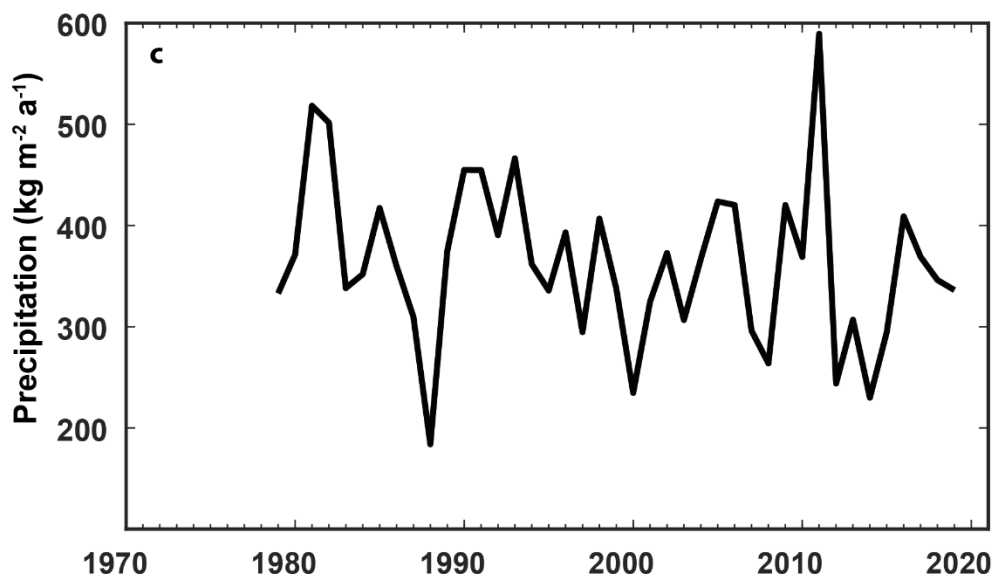
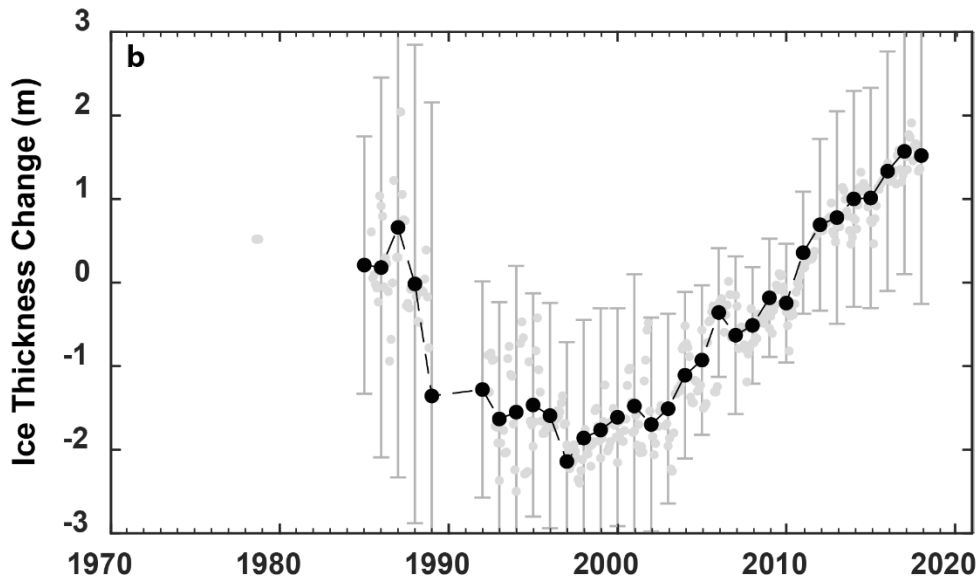
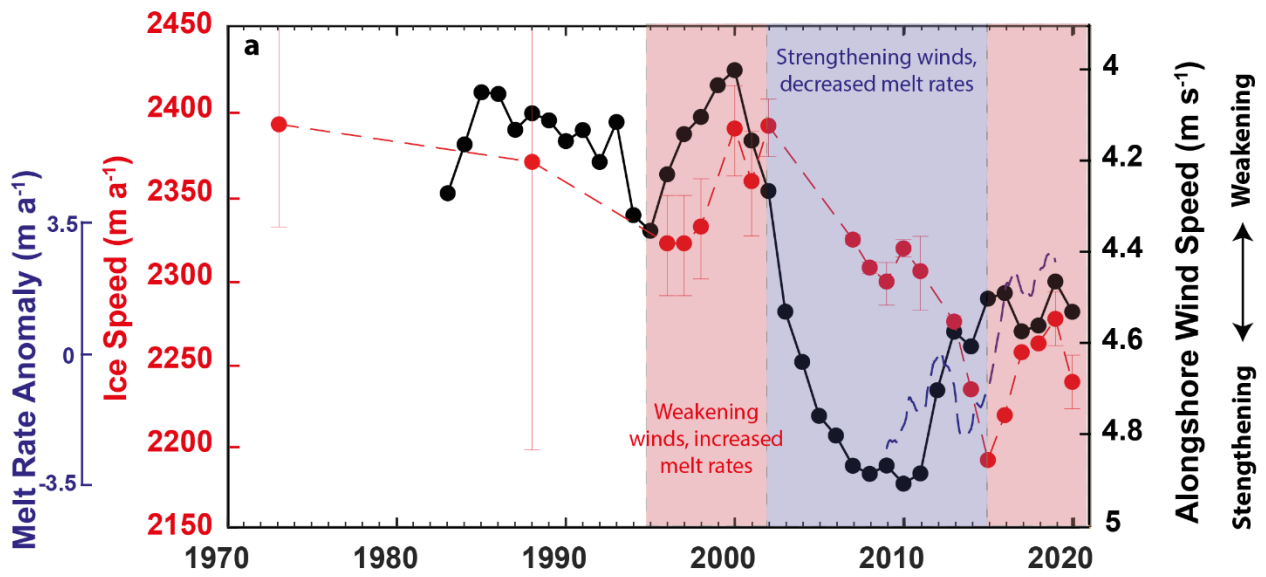
203

204 Ice speed profiles along the transect (T1, Fig. 2a) show a uniform pattern of change across both the  
205 grounded and floating sections of Shirase Glacier (Fig. 2e). At the grounding line, we observe little  
206 change in ice speed between 1973 and 1988, although we note the larger uncertainty in the 1988  
207 estimate of  $\pm 171 \text{ m a}^{-1}$  (Fig. 3ab) and we cannot rule out interannual variations in ice speed within  
208 this date range. Between 1988 and 1996 we observe a  $2 \pm 7\%$  slowdown and a  $2 \pm 1\%$  increase in ice  
209 speed between 1997 and 2000 (Fig. 3a). Post-2000 we observe a slowdown, with an  $8 \pm 1\%$  decrease  
210 in ice speed between 2000 and 2015 (Fig. 3ab). Between 2015 and 2019 ice speed increased by  $4$   
211  $\pm 1\%$  (Fig. 3a). Observations of ice thickness change 20 km inland of the grounding line show a  
212 thinning trend of  $0.27 \pm 0.33 \text{ m a}^{-1}$  between 1987 and 1997, before reversing to a thickening trend of  
213  $0.19 \pm 0.10 \text{ m a}^{-1}$  between 1997 and 2017 (Fig. 3b). There is large interannual variability in  
214 precipitation over Shirase Glacier (Fig. 3c) and no obvious link to observations in ice speed or ice  
215 thickness. Elevation profiles along a section of T1 in 2008, 2013 and 2015 show **a consistent**  
216 seaward migration of the surface slope as it approaches the grounding line (Fig. 2cd, animation S3).  
217 **The absence of any consistent increases in precipitation suggests that this is predominantly a**  
218 **horizontal offset caused by grounding line advance. Therefore, ,which is indicative of grounding line**  
219 **advance and can be visualised in animation S3. b** Between February 2008 and October 2015 we  
220 estimate that the grounding line advanced around 400 m ( $\sim 50 \text{ m yr}^{-1}$ ) from measuring the seaward  
221 displacement of the surface slope, an estimate that is broadly consistent with CryoSat based  
222 observations of seaward grounding line migration between 2010 and 2016 ( $\sim 30 \text{ m a}^{-1}$ ; Konrad et al.,  
223 2018). ~~Observations of ice thickness change 20 km inland of the grounding line show a thinning~~  
224 ~~trend of  $0.27 \pm 0.33 \text{ m a}^{-1}$  between 1987 and 1997, before reversing to a thickening trend of  $0.19 \pm 0.10$~~   
225  ~~$\text{m a}^{-1}$  between 1997 and 2017 (Fig. 3b).~~

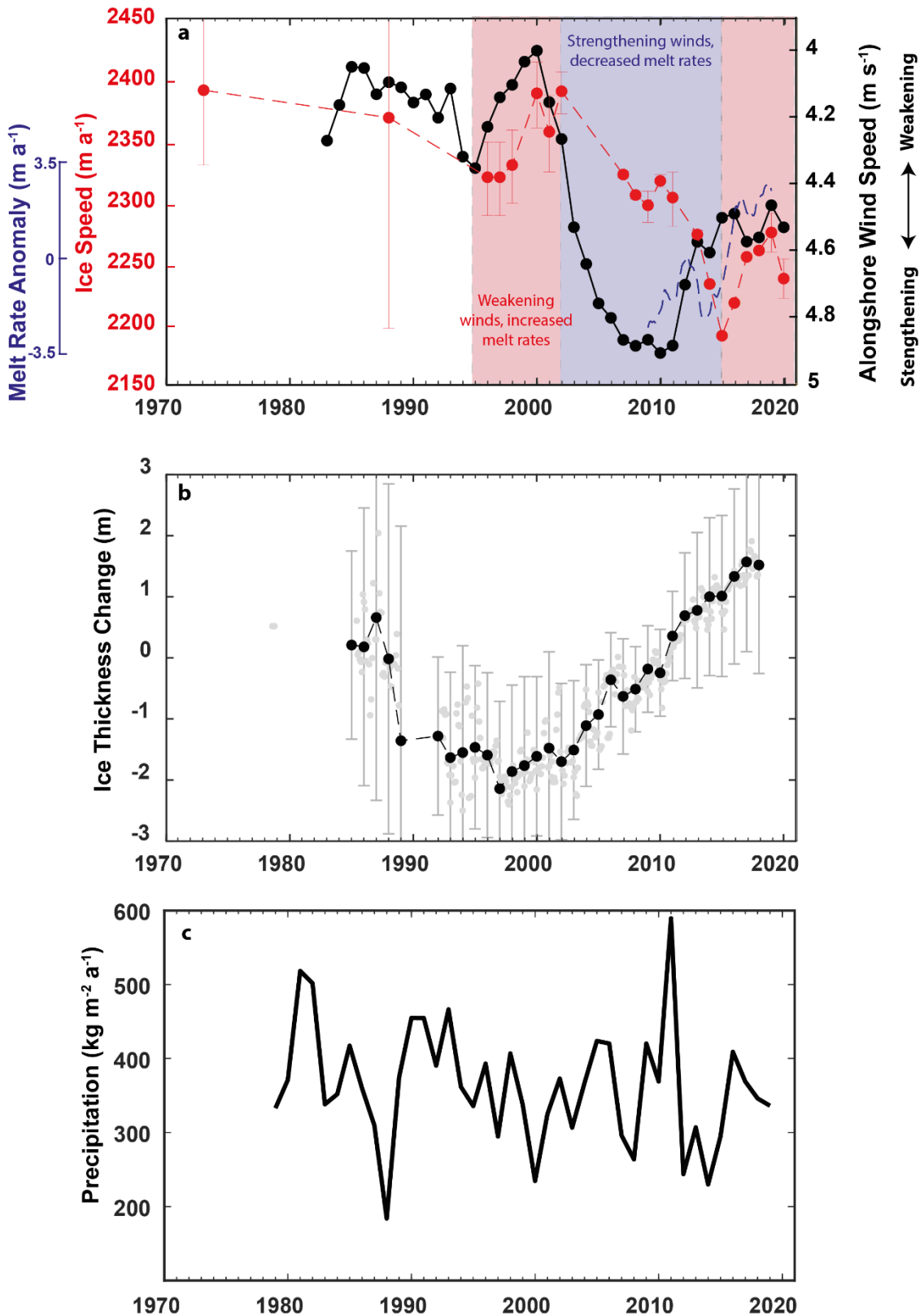
226 ERA5 derived estimates of alongshore easterly wind speed between 1979 and 2020 show limited  
227 variation between 1984 and the early 1990s (Fig. 3a). In the early 1990s there was a small increase  
228 in alongshore wind speed, before a more marked increase from 2000-2010 where alongshore wind  
229 speed increased from around  $4 \text{ m s}^{-1}$  to  $4.8 \text{ m s}^{-1}$  (Fig. 3a). This is before falling slightly to around  $4.5$   
230  $\text{m s}^{-1}$  between 2010 and 2018, which is coincident with an increase in basal melt rate anomalies (Fig.  
231 3a). The multidecadal trend in zonal wind shows a trend for a strengthening of wind in an easterly

232 direction at the continental shelf boundary over much of Enderby Land (Fig. 4). There is no trend in  
233 zonal wind speed over large parts of Dronning Maud Land, with the exception of near Jutulstraumen  
234 Glacier where there is a trend for strengthening wind in the westerly direction (Fig. 4). ~~There is large~~  
235 ~~interannual variability in precipitation over Shirase Glacier (Fig. 3e) and no obvious link to~~  
236 ~~observations in ice speed or ice thickness.~~

237





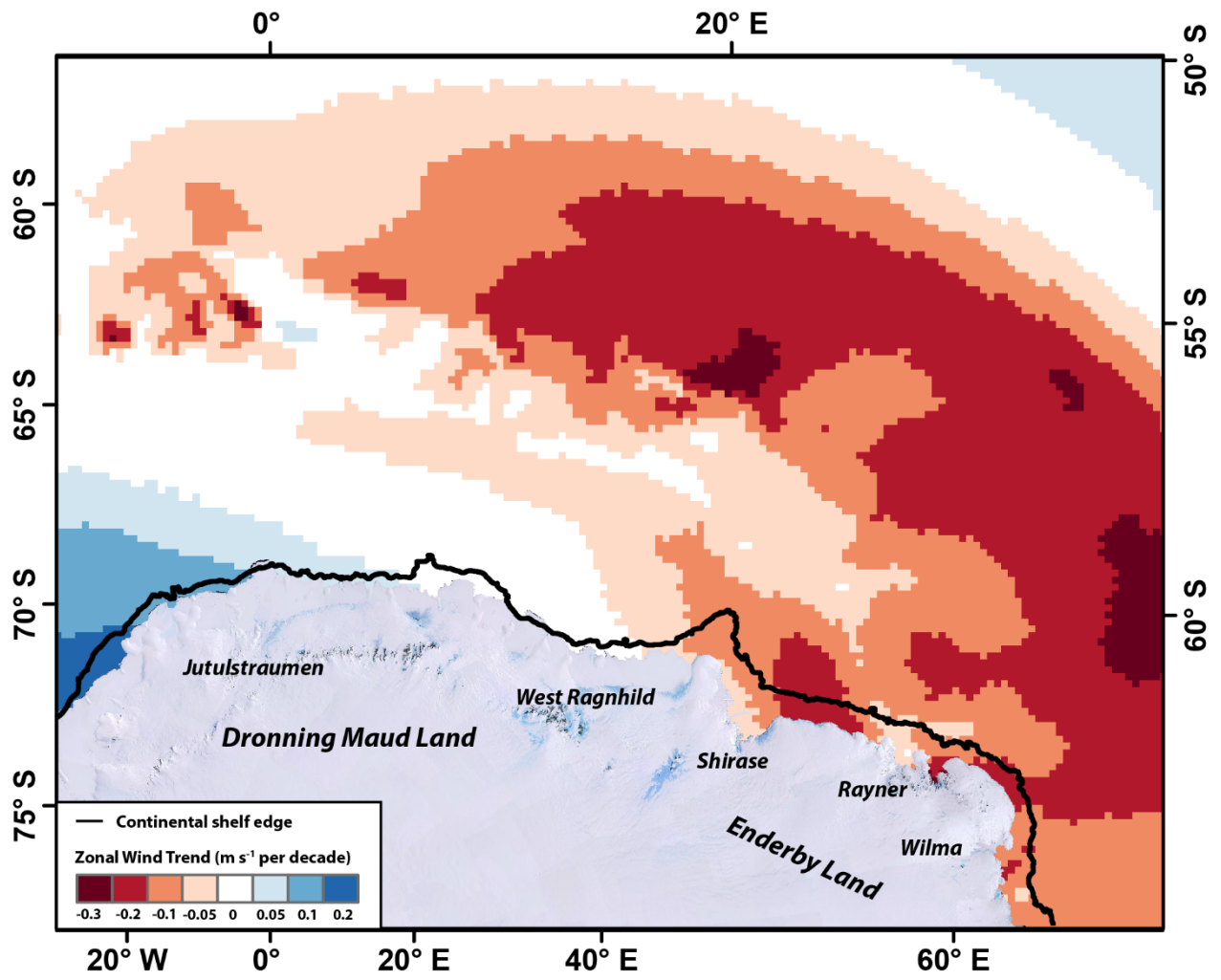


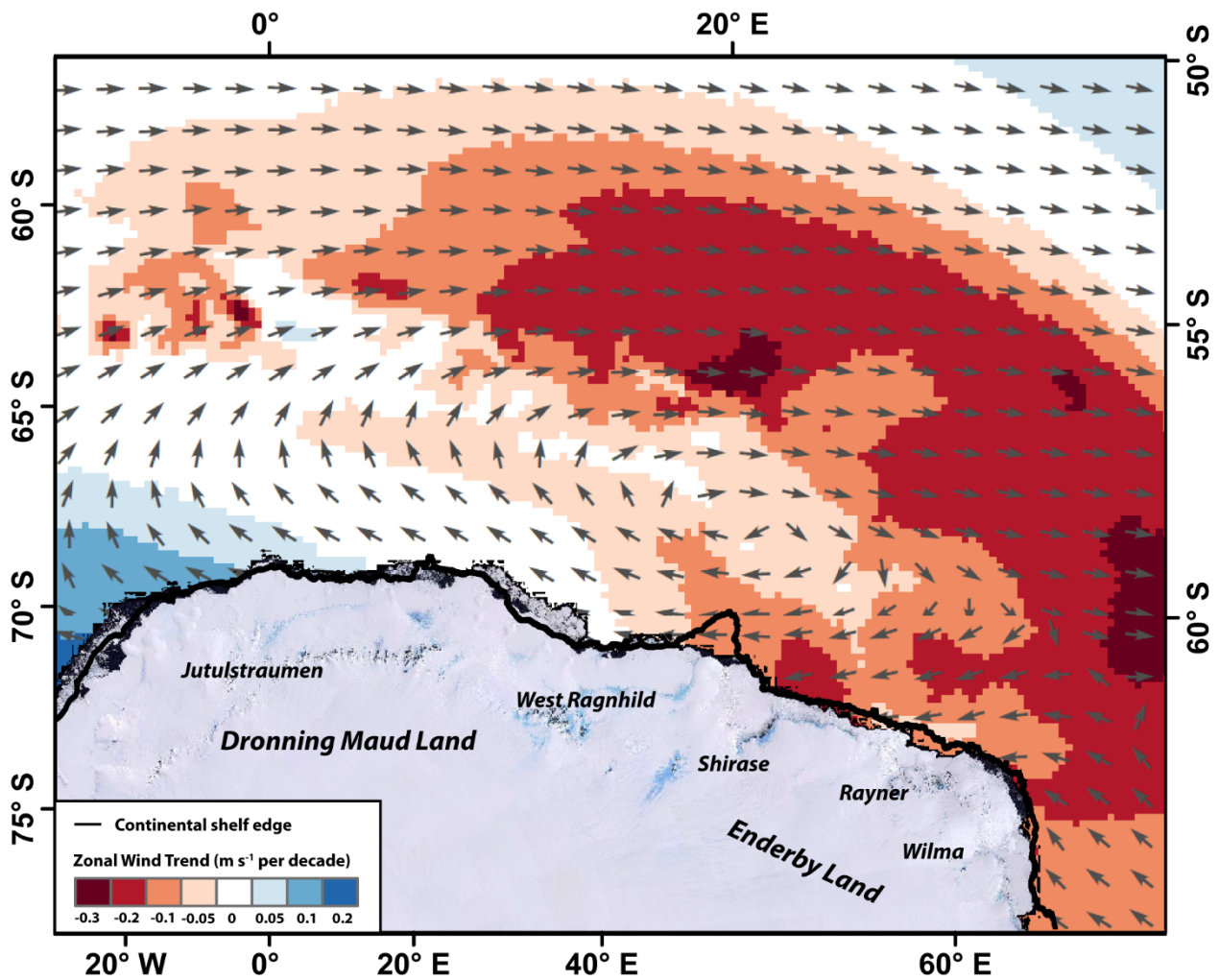
239

240 **Figure 3: a)** Annually averaged ERA5 derived alongshore wind speed from Box A (See Fig. 1) and  
 241 plotted as a 5-year rolling mean (black), ice speed at the Shirase Glacier grounding line along T1  
 242 (red) and modelled melt rate anomaly of the Shirase ice tongue between 2008 and 2018 plotted as a  
 243 1-year rolling mean (blue; Kusahara et al., 2021). Periods of weakening winds cause increased  
 244 mCDW transport, increased basal melt and acceleration. Periods of strengthening winds result in  
 245 relatively less mCDW transport, decreased basal melt rates and glacier slowdown. Note that

246 alongshore wind speed is plotted with an inverted axis. **b)** Annually averaged ice thickness change at  
247 point IT [with respect to 2009/10](#) (see Fig. 2a) extracted from the Schröder et al. (2019) dataset, where  
248 there are at least 6 data points in the calendar year. The error bars are annually averaged errors. The  
249 background grey points are the raw monthly data points. **c)** Annual averaged precipitation over  
250 Shirase Glacier from the MAR regional climate model (Kittel et al., 2021), [uncertainties are not](#)  
251 [provided with these data](#).

252





254

255 **Figure 4:** Linear zonal wind trend 1979-2021 with data smoothed with 60 month moving average  
 256 prior to extracting the trend. Negative values indicate a trend for zonal winds in a more easterly  
 257 direction and positive values indicate a trend for winds in a more westerly direction. **Mean wind**  
 258 **direction (1979-2021) is represented by the grey arrows.** Major outlet glaciers have been labelled.

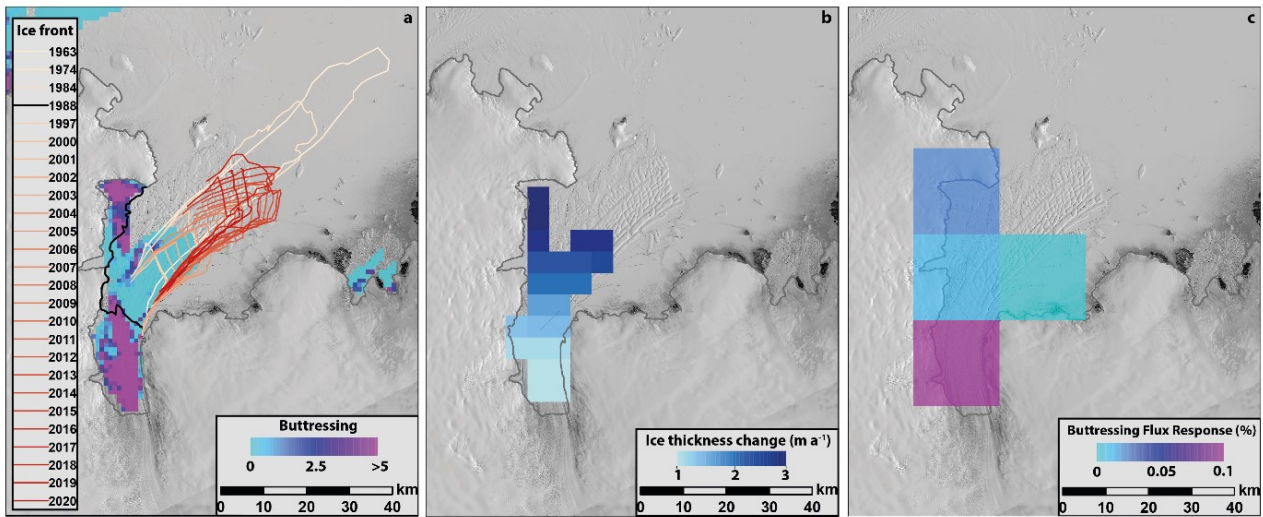
259

## 260 4. Discussion

### 261 4.1 Slowdown and thickening caused by strengthening alongshore winds

262 Calculations indicate that the heavily fractured and unconstrained section of the Shirase ice tongue  
 263 **conglomerate** offers little buttressing force (Fig. 5a; Durrand et al., 2016; Fürst et al., 2016).  
 264 Therefore, it is unlikely that any variations in the extent of the Shirase ice tongue have had a direct  
 265 effect on the ice speed trends we have observed. The only possible exception to this is in 1988 where  
 266 the ice tongue briefly retreated to the edge of its more confined embayment (Fig. 2a), closer to where  
 267 the extent of the ice tongue might be expected to exert buttressing and impact on inland flow speed,  
 268 were it to be removed (Fig. 5a).

269



270

271 **Figure 5: a)** Simulated maximum buttressing potential of the Shirase ice tongue (Durand et al., 2016).  
 272 Light blues mean the ice is passive, purples mean the floating ice is dynamically important. Note how  
 273 the ice tongue conglomerate is not important for buttressing, but parts of the inner shelf are important.  
 274 No dynamically important ice has calved over the past over the past 57 years. **b)** Ice tongue thickness  
 275 change between 2003 and 2019 showing thickening of the Shirase ice tongue (Smith et al., 2020). **c)**  
 276 Simulated response of ice flux to thinning of floating ice in each grid cell by 1 m (Reese et al., 2018),  
 277 the constrained inner tongue near the grounding line is important for buttressing. Note there is no  
 278 change in ice tongue buttressing in response to observed changes in ice tongue extent, but increased  
 279 buttressing expected in response to observed ice tongue thickening. Landsat images are courtesy of  
 280 the U.S. Geological Survey.

281

282 In agreement with previous work, we note that the observed fluctuations in ice tongue extent are  
 283 correlated with landfast sea-ice conditions in Lützow-Holm Bay (Aoki, 2017). Long periods of ice  
 284 tongue advance are associated with persistent landfast sea-ice in Lützow-Holm Bay, while ice tongue  
 285 retreat is associated with landfast sea-ice break-out events removing parts of the ice tongue  
 286 conglomerate (Aoki et al., 2017). ~~These break-out events have occurred sporadically during the~~  
 287 ~~austral summer months (Fig. S1). While there are some sporadic partial break-outs in the landfast~~  
 288 ~~sea-ice during the austral summer months (Fig. S1), there is no evidence of any major changes in fast~~  
 289 ~~ice coverage over the course of our observational time period.~~ It is important to note that fast ice only  
 290 helps control the length of the ice tongue conglomerate (Fig. 1b) and ~~it is unlikely there is no evidence~~  
 291 that the fast ice has any major role in providing buttressing for Shirase Glacier. For example, we note  
 292 that there was no obvious increase in ice speed at the grounding line or over the inner ice tongue in  
 293 1988 when the fast ice and ice tongue conglomerate were completely removed from the bay (Fig. 2a,  
 294 S13), ~~albeit there are large uncertainties in our 1988 ice speed estimate ( $\pm 171 \text{ m a}^{-1}$ ).~~ In addition,  
 295 Nakamura et al. (2010) recorded only a very modest  $20 \pm 30 \text{ m a}^{-1}$  ( $0.8 \pm 1.3 \%$ ) change in ice speed  
 296 at the grounding line after a partial fast ice break-out event in 1998, ~~and there was also an~~

297 indistinguishable change in ice speed at the grounding line following a break-out in 2017 (Nakamura  
298 et al., 2022).

299 Point IT, 20 km inland of the Shirase Glacier grounding line was thinning at a rate of  $-0.27 \pm 0.33$  m  
300  $\text{a}^{-1}$  between 1987 and 1997 (Fig. 3be), a pattern consistent with field observations up to 200 km further  
301 inland in the 1960s, 1970s and 1980s (Mae and Naruse, 1978; Naruse, 1979; Nisho et al., 1989; Toh  
302 and Shibuya, 1992). However, in  $\sim 2000$  there was a slowdown in Shirase Glacier (Fig. 3a) and this  
303 thinning trend reversed to thickening (Fig. 3b). This slowdown and thickening coincides with an  
304 increase in alongshore easterly wind speed adjacent to the Shirase coastline (Fig. 3a). The seasonal  
305 strengthening in alongshore easterly winds offshore of the Shirase coastline has been observed to  
306 deepen the thermocline in Lützow-Holm Bay, limiting the inflow of mCDW onto the continental  
307 shelf and reduce basal melt rates (Hirano et al., 2020). We suggest that this same process over annual  
308 to decadal timescales has caused the slowdown of Shirase Glacier.

309 Increased alongshore wind speed from  $\sim 2000$  enhanced Ekman convergence at the coast, deepening  
310 the thermocline with a short lag and inhibited the inflow of warm mCDW into Lützow-Holm Bay.  
311 The subsequent cooling of Lützow-Holm Bay reduced the basal melt rate of the Shirase ice tongue.  
312 This reduction in basal melt caused the ice tongue to thicken and is confirmed by ICESat and ICESat-  
313 2 observations of the of the Shirase ice tongue that show a mean thickening of  $1.87$  m  $\text{yr}^{-1}$  from 2003-  
314 2019 (Fig. 5b; Smith et al., 2020). Instantaneous numerical modelling experiments show that ice  
315 discharge is sensitive to thickness changes in the inner ice tongue (Reese et al., 2018; Fig. 5c).  
316 Therefore, the dynamic thickening of the inner ice tongue would be expected to increase buttressing  
317 through time (Fig. 5c) and ultimately drive the overall slowdown in ice speed, grounding line advance  
318 and inland thickening that we observe. Importantly, our results show that wind-driven ocean forcing  
319 is also contributing to mass gain in the Lützow-Holm Bay. This is likely in addition to surface mass  
320 balance processes, as indicated by the widespread inland thickening of the Shirase catchment between  
321 2003 and 2019 (Smith et al., 2020). However, there is no evidence of a long-term increase in  
322 precipitation at the Shirase catchment (Fig. 3c). Instead the inland thickening is likely a consequence  
323 of extreme anomalous snowfall events in 2009 and 2011 ~~in addition to surface mass balance processes~~  
324 ~~across the wider region~~ (e.g. Boening et al., 2012; Lenaerts et al., 2013).

325 Within the longer-term slowdown of Shirase Glacier between 1973 and 2020 we observe brief periods  
326 of acceleration in response to short-lived periods of weakening alongshore winds. For example, both  
327 of the accelerations in ice speed from 1997-2000 and 2015-2019 are preceded by brief periods of  
328 weakening alongshore winds (Fig. 3a). These periods of weakening alongshore winds cause relatively  
329 higher basal melt rates because they raise the thermocline closer to the ocean surface and enable a  
330 greater influx of mCDW into Lützow-Holm Bay (Hirano et al., 2020). This is supported by the close



331 relationship between alongshore wind speed and modelled melt rate anomalies (Fig. 3a; Kusahara et  
332 al., 2021). ~~However, we would not expect a perfect relationship between alongshore wind, melt rates~~  
333 ~~and ice speed particularly over short interannual timescales. For example, an increase in melt rates~~  
334 ~~could cause the ice tongue to thin and accelerate or simply thicken at a lower rate and continue to~~  
335 ~~slowdown.~~ Although we do note some slight discrepancies in this relationship, for example between  
336 2008 and 2011, changes in melt rates precede changes in winds. This could be related to the relative  
337 smoothing of both datasets, with alongshore wind plotted as a 5-year rolling mean and melt rates  
338 plotted as a 1-year rolling mean.

339 The interannual variability in ice flow speed at Shirase Glacier in response to wind-forced ocean  
340 variability is analogous to other regions of Antarctica where mCDW periodically floods the  
341 continental shelf e.g. Pine Island (Christianson et al., 2016), Thwaites (Miles et al., 2020) and Totten  
342 glaciers (Greene et al., 2017). The pattern of change at Shirase Glacier is unique, however, in that it  
343 is the only outlet glacier in Antarctica with a warm water regime that has been observed to be slowing  
344 down and thickening during the 21<sup>st</sup> century, as opposed to accelerating and thinning (e.g. Mouginit  
345 et al., 2014; Greene et al., 2017). As such, our results highlight that this oceanic mode of ice melt is  
346 not universally associated with mass loss in Antarctica.

347

#### 348 **4.2 Wider links to climate forcing and future implications**

349 In response to both increased greenhouse gas emissions and ozone depletion (Thompson et al., 2011;  
350 Wang et al., 2014; Perren et al., 2020) the band of mid-latitude westerly winds that encircle Antarctica  
351 have both strengthened and migrated southwards towards the ice sheet over recent decades  
352 (Thompson & Solomon, 2002; Marshall, 2003; Turner, 2005; Bracegirdle et al., 2018). In the  
353 Amundsen Sea sector of West Antarctica, this anthropogenically-driven migration has been linked to  
354 westerly wind anomalies over the continental shelf (Holland et al., 2019), which have enabled a  
355 greater influx of warm mCDW onto the continental shelf and have driven enhanced localized ice  
356 sheet mass loss (Thoma et al., 2008). At Shirase Glacier, our observations of strengthening alongshore  
357 easterly winds suggest any southward encroachment of the mid-latitude westerlies has yet to impact  
358 the Shirase coastline. This may also be the case for parts of the wider Enderby Land coastlines where  
359 alongshore easterlies ~~have also been observed to~~ have strengthened along the continental shelf edge  
360 (Hazel & Stewart, 2019). However, it remains unknown what effect these strengthening easterly  
361 winds may have had on other nearby outlet glaciers (e.g. Rayner and Wilma; Fig. 4), which are yet  
362 to be studied in detail. The trend in strengthening alongshore easterlies might also be linked to  
363 enhanced katabatic winds as low pressure systems track progressively further south and enhance the

364 pole to coast pressure gradient (Hazel & Stewart, 2019). It is unclear if the enhancement of the pole-  
365 to-coast pressure gradient has been influenced by the anthropogenically-driven southerly migration  
366 of the mid-latitude westerlies, or if it has been caused by inherent natural decadal variability within  
367 the system.

368 Over the course of the 21<sup>st</sup> century, the southerly migration of the mid-latitude westerlies is projected  
369 to continue in a warming climate (Yin, 2005; Perren et al., 2020). Along the Shirase coastline, this  
370 continued southerly migration may ultimately result in a similar situation to the Amundsen Sea, such  
371 that westerly wind anomalies offshore would result in enhanced mCDW transport into Lützow-Holm  
372 Bay and cause mass loss. Alternatively, the westerly winds may never migrate close enough to the  
373 Shirase coastline to impact alongshore winds, and instead, alongshore winds may continue to  
374 strengthen as the pole to coast pressure gradient increases. This would result in further cooling of  
375 Lützow-Holm Bay and ice tongue thickening, and further mass gain. In a wider context, an improved  
376 understanding of the potential changes in ocean forcing in response to broader atmospheric patterns  
377 expected over the coming decades is needed in the Enderby and Dronning Maud Land sectors.

378

## 379 **5. Conclusion**

380 Our observations of Shirase Glacier are a rare example of a glacier reversing a trend of mass loss  
381 from at least the 1970s-1990s to mass gain over the last two decades. As far as we are aware this is  
382 the only major fast flowing Antarctic outler glacier to display this pattern of behaviour. This reversal  
383 has been driven by a slowdown of the Shirase Glacier upstream of the grounding line in response to  
384 strengthening alongshore **easterly** winds that have limited the inflow of warm mCDW into Lützow-  
385 Holm Bay, reduced basal melt rates, and caused its ice tongue to dynamically thicken. Should this  
386 strengthening of alongshore easterly winds continue into the future, the Shirase catchment will  
387 continue to experience a positive mass balance due to both the slow-down in ice discharge, and to the  
388 predicted increase in precipitation in response to atmospheric warming (e.g. Ligtenberg et al., 2013;  
389 Kittel et al., 2021). Our results highlight the need for a greater consideration of the potential role of  
390 ocean forcing in both the current and future mass balance of the wider Enderby and Dronning Maud  
391 Land regions.

392

## 393 **Data Availability**

394 Landsat and ARGON imagery was provided free of charge by the US Geological Survey Earth  
395 Resources Observation Science Center (<https://earthexplorer.usgs.gov/>). For the MODIS imagery we

396 also acknowledge the use of imagery from the NASA Worldview application  
397 (<https://worldview.earthdata.nasa.gov>), part of the NASA Earth Observing System Data and  
398 Information System (EOSDIS). Cosi-corr is an ENVI plug-in and can be downloaded from  
399 [http://www.tectonics.caltech.edu/slip\\_history/spot\\_coseis/download\\_software.html](http://www.tectonics.caltech.edu/slip_history/spot_coseis/download_software.html). The ITS\_LIVE  
400 velocity products are available from <https://doi.org/10.5067/IMR9D3PEI28U>. GoLIVE velocity  
401 products are available from <http://dx.doi.org/10.7265/N5ZP442B>. ERA5 data is available from  
402 <https://doi.org/10.24381/cds.adbb2d47>. Wind data from Syowa station is available via the SCAR  
403 READER at <http://dx.doi.org/10.5285/569d53fb-9b90-47a6-b3ca-26306e696706>. The MOA  
404 grounding line product is available at <https://doi.org/10.7265/N5KP8037>. BedMachine is available at  
405 <https://doi.org/10.5067/E1QL9HFQ7A8M>. The ice shelf thickness change dataset from Smith et al.  
406 (2020) is available at <http://hdl.handle.net/1773/45388>. REMA DEM strips are available at  
407 <https://www.pgc.umn.edu/data/rema/>. Lützow-Holm Bay bathymetry is available at  
408 <https://doi.org/10.17632/z6w4xd6s3s.1>. The RAMP mosaic is available at <https://doi.org/10.5067/8AF4ZRPULS4H>. Ice shelf extent buttressing dataset from Durand et al., 2016 is available at  
409 <https://doi.org/10.5067/FWHORAYVZCE7>. SPIRIT DEM's are available from  
410 <https://theia.cnes.fr/atdistrib/rocket/#/search?collection=Spirit>. MAR precipitation data is available  
411 from <https://doi.org/10.5281/zenodo.4459259>.

413

#### 414 **Acknowledgements**

415 This research has been supported by a UK Natural Environment Research Council (NERC) grant  
416 (NE/R000824/1). BM was also supported by a Leverhulme Early Career Fellowship (ECF-2021-  
417 484). Hersbach, H. et al.'s (2018) dataset was downloaded from the Copernicus Climate Change  
418 Service (C3S) Climate Data Store. We acknowledge the DEMs provided by the Byrd Polar and  
419 Climate Research Center and the Polar Geospatial Center under NSF-OPP awards 1543501, 1810976,  
420 1542736, 1559691, 1043681, 1541332, 0753663, 1548562, 1238993 and NASA award  
421 NNX10AN61G. Computer time provided through a Blue Waters Innovation Initiative. DEMs  
422 produced using data from Maxar. We thank Ronja Reese for providing the ice flux buttressing  
423 response dataset. We would like to thank two anonymous reviewers, along with the editor Etienne  
424 Berthier, for providing constructive comments which led to the improvement of this paper.

425

426 **Author contributions:** All authors contributed to the design of the study. BWJM collected and  
427 analysed the remote sensing data and led the manuscript writing with input from all authors.

428

429 **Competing interests:** The authors declare no competing interests

431 **References**

- 432 Aoki, S., Ozawa, T. & Doi, K. ~~(2000)~~: GPS observation of the sea level variation in Lützow-Holm  
 433 Bay, Antarctica. *Geophysical Research Letters*, 27(15), 2285-2288.  
 434 <https://doi.org/10.1029/1999GL011304>, 2000.
- 435 Aoki, S. ~~(2017)~~: Breakup of land-fast sea ice in Lützow-Holm Bay, East Antarctica, and its  
 436 teleconnection to tropical Pacific sea surface temperatures. *Geophysical Research Letters*,  
 437 44(7), 3219–3227. <https://doi.org/10.1002/2017GL072835>, 2017.
- 438 Aoyama, Y., Doi, K., Shibuya, K., Ohta, H., & Tsuwa, I.: ~~(2013)~~-Near real-time monitoring of flow  
 439 velocity and direction in the floating ice tongue of the Shirase Glacier using low-cost GPS  
 440 buoys. *Earth, Planets and Space*, 65(2), 103–108. <https://doi.org/10.5047/EPS.2012.06.011>,  
 441 2013.
- 442 Boening, C., Lebsack, M., Landerer, F., & Stephens, G. ~~(2012)~~: Snowfall-driven mass change on  
 443 the East Antarctic ice sheet. *Geophysical Research Letters*, 39(21).  
 444 <https://doi.org/10.1029/2012GL053316>, 2012.
- 445 Bracegirdle, T. J., Hyder, P., & Holmes, C. R. ~~(2018)~~: CMIP5 Diversity in Southern Westerly Jet  
 446 Projections Related to Historical Sea Ice Area: Strong Link to Strengthening and Weak Link to  
 447 Shift. *Journal of Climate*, 31(1), 195–211. <https://doi.org/10.1175/JCLI-D-17-0320.1>, 2018.
- 448 Brunt, K. M., Fricker, H. A., Padman, L., Scambos, T. A., & O’Neel, S. ~~(2010)~~: Mapping the  
 449 grounding zone of the Ross Ice Shelf, Antarctica, using ICESat laser altimetry. *Annals of*  
 450 *Glaciology*, 51(55), 71–79. <https://doi.org/10.3189/172756410791392790>, 2010.
- 451 Christianson, K., Bushuk, M., Dutrieux, P., Parizek, B. R., Joughin, I. R., Alley, R. B., et al.  
 452 ~~(2016)~~: Sensitivity of Pine Island Glacier to observed ocean forcing. *Geophysical Research*  
 453 *Letters*, 43(20), 10,817-10,825. <https://doi.org/10.1002/2016GL070500>, 2016.
- 454 Cook, A. J., Holland, P. R., Meredith, M. P., Murray, T., Luckman, A., & Vaughan, D. G.: ~~(2016)~~.  
 455 Ocean forcing of glacier retreat in the western Antarctic Peninsula. *Science*, 353(6296), 283–  
 456 286, 2016.-
- 457 Durand, G., F. Gillet-Chaulet, O. Gagliardini, and J. J. Fürst.: ~~(2016)~~. SUMER Antarctic Ice-shelf  
 458 Buttressing, Version 1. Boulder, Colorado USA. NASA National Snow and Ice Data Center  
 459 Distributed Active Archive Center. <https://doi.org/10.5067/FWHORAYVZCE7>, 2016.-
- 460 Fahnestock, M., Scambos, T., Moon, T., Gardner, A., Haran, T., & Klinger, M.: ~~(2016)~~. Rapid  
 461 large-area mapping of ice flow using Landsat 8. *Remote Sensing of Environment*, 185, 84–94.  
 462 <https://doi.org/10.1016/J.RSE.2015.11.023>, 2016.
- 463 Fricker, H. A., Coleman, R., Padman, L., Scambos, T. A., Bohlander, J., & Brunt, K. M.: ~~(2009)~~.  
 464 Mapping the grounding zone of the Amery Ice Shelf, East Antarctica using InSAR, MODIS  
 465 and ICESat. *Antarctic Science*, 21(5), 515–532. <https://doi.org/10.1017/S095410200999023X>,  
 466 2009.
- 467 Fürst, J. J., Durand, G., Gillet-Chaulet, F., Tavaré, L., Rankl, M., Braun, M., & Gagliardini, O.  
 468 ~~(2016)~~: The safety band of Antarctic ice shelves. *Nature Climate Change*, 6(5), 479–482.  
 469 <https://doi.org/10.1038/nclimate2912>, 2016.

- 470 Gardner, A., Fahnestock, M., & Scambos, T. A. ~~(2020)~~: ITS\_LIVE Regional Glacier and Ice Sheet  
471 Surface Velocities. <https://doi.org/doi:10.5067/6II6VW8LLWJ7>, 2020.
- 472 Gardner, A. S., Moholdt, G., Scambos, T., Fahnestock, M., Ligtenberg, S., van den Broeke M., &  
473 Nilsson, J. ~~(2018)~~: Increased West Antarctic and unchanged East Antarctic ice discharge over  
474 the last 7 years. *Cryosphere*, 12(2), 521–547. <https://doi.org/10.5194/TC-12-521-2018>, 2018.
- 475 Greene, C. A., Blankenship, D. D., Gwyther, D. E., Silvano, A., & van Wijk, E. ~~(2017)~~: Wind  
476 causes Totten Ice Shelf melt and acceleration. *Science Advances*, 3(11), e1701681–e1701681.  
477 <https://doi.org/10.1126/sciadv.1701681>, 2017.
- 478 Haran, T., J. Bohlander, T. Scambos, T. Painter, and M. Fahnestock. ~~(2019)~~, updated 2019:  
479 MODIS Mosaic of Antarctica 2008-2009 (MOA2009) Image Map, Version 2. Boulder,  
480 Colorado USA. NASA National Snow and Ice Data Center Distributed Active Archive Center.  
481 doi: <https://doi.org/10.5067/4ZL43A4619AF>, 2019.
- 482 Hazel, J. E., & Stewart, A. L. ~~(2019)~~: Are the Near-Antarctic Easterly Winds Weakening in  
483 Response to Enhancement of the Southern Annular Mode? *Source: Journal of Climate*, 32(6),  
484 1895–1918. <https://doi.org/10.2307/26663209>, 2019.
- 485 Hersbach, H., Bell, B., Berrisford, P., Hirahara, S., Horányi, A., Muñoz-Sabater, J., et al.: ~~(2020)~~  
486 The ERA5 global reanalysis. *Quarterly Journal of the Royal Meteorological Society*, 146(730),  
487 1999–2049. <https://doi.org/10.1002/QJ.3803>, 2020.
- 488 Heid, T., & Kääb, A. ~~(2012)~~: Evaluation of existing image matching methods for deriving glacier  
489 surface displacements globally from optical satellite imagery. *Remote Sensing of*  
490 *Environment*, 118, 339–355. <https://doi.org/10.1016/J.RSE.2011.11.024>, 2012.
- 491 Hirano, D., Tamura, T., Kusahara, K., Ohshima, K. I., Nicholls, K. W., Ushio, S., et al.: ~~(2020)~~  
492 Strong ice-ocean interaction beneath Shirase Glacier Tongue in East Antarctica. *Nature*  
493 *Communications* 2020 11:1, 11(1), 1–12. <https://doi.org/10.1038/s41467-020-17527-4>, 2020.
- 494 Holland, P. R., Bracegirdle, T. J., Dutrieux, P., Jenkins, A., & Steig, E. J. (2019). West Antarctic ice  
495 loss influenced by internal climate variability and anthropogenic forcing. *Nature Geoscience*  
496 2019 12:9, 12(9), 718–724. <https://doi.org/10.1038/s41561-019-0420-9>
- 497 Howat, I. M., Porter, C., Smith, B. E., Noh, M. J., & Morin, P. ~~(2019)~~: The reference elevation  
498 model of Antarctica. *Cryosphere*, 13(2), 665–674. <https://doi.org/10.5194/TC-13-665-2019>,  
499 2019.
- 500 Jacobs, S. S., Helmer, H. H., Doake, C. S. M., Jenkins, A., & Frolich, R. M. ~~(1992)~~: Melting of ice  
501 shelves and the mass balance of Antarctica. *Journal of Glaciology*, 38(130), 375–387.  
502 <https://doi.org/10.3189/S0022143000002252>, 1992.
- 503 Jenkins, A., Shoosmith, D., Dutrieux, P., Jacobs, S., Kim, T. W., Lee, S. H., et al. ~~(2018)~~: West  
504 Antarctic Ice Sheet retreat in the Amundsen Sea driven by decadal oceanic variability, 11(10),  
505 733–738. <https://doi.org/10.1038/s41561-018-0207-4>, 2018.
- 506 Jezek, K. C., J. C. Curlander, F. Carsey, C. Wales, and R. G. Barry. ~~(2013)~~: RAMP AMM-1 SAR  
507 Image Mosaic of Antarctica, Version 2. Boulder, Colorado USA. NASA National Snow and  
508 Ice Data Center Distributed Active Archive Center. <https://doi.org/10.5067/8AF4ZRPULS4H>,  
509 2013.

- 510 Kameda, T., Nakawo, M., Mae, S., Watanabe, O., & Naruse, R.: ~~(1990)~~. Thinning of the Ice Sheet  
511 Estimated from Total Gas Content of Ice Cores in Mizuho Plateau, East Antarctica. *Annals of*  
512 *Glaciology*, 14, 131–135. <https://doi.org/10.3189/S0260305500008429>, 1990.
- 513 Kittel, C., Amory, C., Agosta, C., Jourdain, N. C., Hofer, S., Delhasse, A., et al.: ~~(2021)~~:- Diverging  
514 future surface mass balance between the Antarctic ice shelves and grounded ice sheet.  
515 *Cryosphere*, 15(3), 1215–1236. <https://doi.org/10.5194/TC-15-1215-2021>, 2021.
- 516 Konrad, H., Shepherd, A., Gilbert, L., Hogg, A. E., McMillan, M., Muir, A., & Slater, T.: ~~(2018)~~:-  
517 Net retreat of Antarctic glacier grounding lines. *Nature Geoscience*, 11(4), 258–262.  
518 <https://doi.org/10.1038/s41561-018-0082-z>, 2018.
- 519 Korona, J., Berthier, E., Bernard, M., Rémy, F and Thouvenot, E.: ~~(2009)~~ ISPRS Journal of  
520 Photogrammetry and Remote Sensing SPIRIT. SPOT 5 stereoscopic survey of Polar Ice:  
521 reference images and topographies during the fourth International Polar Year (2007–2009).  
522 ISPRS Journal of Photogrammetry and Remote Sensing 64(2), 204–212. doi:  
523 10.1016/j.isprsjprs.2008.10.005, 2009.-
- 524 Kusahara, K., Hirano, D., Fujii, M., D. Fraser, A., & Tamura, T.: ~~(2021)~~:- Modeling intensive ocean-  
525 cryosphere interactions in Lützow-Holm Bay, East Antarctica. *Cryosphere*, 15(4), 1697–1717.  
526 <https://doi.org/10.5194/TC-15-1697-2021>, 2021
- 527 Lenaerts, J. T. M., van Meijgaard, E., van den Broeke, M. R., Ligtenberg, S. R. M., Horwath, M., &  
528 Isaksson, E.: ~~(2013)~~:- Recent snowfall anomalies in Dronning Maud Land, East Antarctica, in a  
529 historical and future climate perspective. *Geophysical Research Letters*, 40(11), 2684–2688.  
530 <https://doi.org/10.1002/GRL.50559>, 2013.
- 531 Leprince, S., Ayoub, F., Klinger, Y., & Avouac, J.-P.: ~~(2007)~~:- *Co-Registration of Optically Sensed*  
532 *Images and Correlation (COSI-Corr): an Operational Methodology for Ground Deformation*  
533 *Measurements*. Igarss: 2007 Ieee International Geoscience and Remote Sensing Symposium,  
534 1–12,1943–1946. <https://doi.org/10.1109/Igarss.2007.4423207>, 2007.
- 535 Ligtenberg, S. R. M., van de Berg, W. J., van den Broeke, M. R., Rae, J. G. L., & van Meijgaard, E.:  
536 ~~(2013)~~:- Future surface mass balance of the Antarctic ice sheet and its influence on sea level  
537 change, simulated by a regional atmospheric climate model. *Climate Dynamics*, 41(3–4), 867–  
538 884. <https://doi.org/10.1007/S00382-013-1749-1>, 2013.
- 539 Mae, S., & Naruse, R. : ~~(1978)~~. Possible causes of ice sheet thinning in the Mizuho Plateau. *Nature*  
540 1978 273:5660, 273(5660), 291–292. <https://doi.org/10.1038/273291a0>, 1978.
- 541 Marshall, G.: ~~(2003)~~. Trends in the Southern Annular Mode from observations and reanalyses. *J.*  
542 *Clim.*, 16, 4134–4143, 2003.-
- 543 Miles, B. W. J. J., Stokes, C. R., Jenkins, A., Jordan, J. R., Jamieson, S. S. R. R., & Gudmundsson,  
544 G. H.: ~~(2020)~~. Intermittent structural weakening and acceleration of the Thwaites Glacier  
545 Tongue between 2000 and 2018. *Journal of Glaciology*, 1–11.  
546 <https://doi.org/10.1017/jog.2020.20>, 2020.
- 547 Moriwaki, K., & Yoshida, Y.: ~~(1983)~~. Submarine topography of Lützow-Holm Bay, Antarctica.  
548 *Mem. Natl. Inst. Polar Res.*, 28, 247–258, 1983.-
- 549 Morlighem, M.: ~~(2020)~~. MEaSUREs BedMachine Antarctica, Version 2. Boulder, Colorado USA.  
550 NASA National Snow and Ice Data Center Distributed Active Archive Center. doi:  
551 <https://doi.org/10.5067/E1QL9HFQ7A8M>, 2020.-



- 552 Morlighem, M., Rignot, E., Binder, T., Blankenship, D., Drews, R., Eagles, G., et al. ~~(2020)~~: Deep  
553 glacial troughs and stabilizing ridges unveiled beneath the margins of the Antarctic ice sheet.  
554 *Nature Geoscience*, 13(2), 132–137. <https://doi.org/10.1038/s41561-019-0510-8>, 2020.
- 555 Mouginit, J., Rignot, E., & Scheuchl, B.: ~~(2014)~~. Sustained increase in ice discharge from the  
556 Amundsen Sea Embayment, West Antarctica, from 1973 to 2013. *Geophysical Research*  
557 *Letters*, 41(5), 1576–1584. <https://doi.org/10.1002/2013GL059069>, 2014.
- 558 Nakamura, K., Doi, K., & Shibuya, K.: ~~(2007)~~. Estimation of seasonal changes in the flow of  
559 Shirase Glacier using JERS-1/SAR image correlation. *Polar Science*, 1(2–4), 73–83.  
560 <https://doi.org/10.1016/J.POLAR.2007.09.002>, 2007.
- 561 Nakamura, K., Doi, K., & Shibuya, K.: ~~(2010)~~. Fluctuations in the flow velocity of the Antarctic  
562 Shirase Glacier over an 11-year period. *Polar Science*, 4(3), 443–455.  
563 <https://doi.org/10.1016/J.POLAR.2010.04.010>, 2010.
- 564 Nakamura, K., Aoki, S., Yamanokuchi, T., and Tamura, T.: Interactive movements of outlet glacier  
565 tongue and landfast sea ice in Lützow-Holm Bay, East Antarctica, detected by ALOS-  
566 2/PALSAR-2 imagery. *Science of Remote Sensing*, 6, 100064.  
567 <https://doi.org/10.1016/j.srs.2022.100064>, 2022.
- 568 Naruse, R.: ~~(1979)~~. Thinning of the Ice Sheet in Mizuho Plateau, East Antarctica. *Journal of*  
569 *Glaciology*, 24(90), 45–52. <https://doi.org/10.3189/S0022143000014635>, 1979.
- 570 Nishio, F., Mae, S., Ohmae, H., Takahashi, S., Nakawo, M., & Kawada, K.: ~~(1989)~~. Dynamical  
571 behaviour of the ice sheet in Mizuho Plateau, East Antarctica. *Proc. NIPR Symp. Polar*  
572 *Meteorol. Glaciol.*, 2, 97–104, 1989.-
- 573 Ohshima, K. I., Takizawa, T., Ushio, S., & Kawamura, T.: ~~(1996)~~. Seasonal variations of the  
574 Antarctic coastal ocean in the vicinity of Lützow-Holm Bay. *Journal of Geophysical Research*  
575 *C: Oceans*, 101(C9), 20617–20628. <https://doi.org/10.1029/96JC01752>, 1996.
- 576 Pattyn, F., & Derauw, D.: ~~(2002)~~. Ice-dynamic conditions of Shirase Glacier, Antarctica, inferred  
577 from ERS SAR interferometry. *Journal of Glaciology*, 48(163), 559–565.  
578 <https://doi.org/10.3189/172756502781831115>, 2002.
- 579 Pattyn, F., & Naruse, R.: ~~(2003)~~. The nature of complex ice flow in Shirase Glacier catchment, East  
580 Antarctica. *Journal of Glaciology*, 49(166), 429–436.  
581 <https://doi.org/10.3189/172756503781830610>, 2003.
- 582 Perren, B. B., Hodgson, D. A., Roberts, S. J., Sime, L., van Nieuwenhuyze, W., Verleyen, E., &  
583 Vyverman, W.: ~~(2020)~~. Southward migration of the Southern Hemisphere westerly winds  
584 corresponds with warming climate over centennial timescales. *Communications Earth &*  
585 *Environment* 2020 1:1, 1(1), 1–8. <https://doi.org/10.1038/s43247-020-00059-6>, 2020.
- 586 Reese, R., Gudmundsson, G. H., Levermann, A., & Winkelmann, R.: ~~(2018)~~. The far reach of ice-  
587 shelf thinning in Antarctica. *Nature Climate Change*, 8(1), 53– 57.  
588 <https://doi.org/10.1038/s41558-017-0020-x>, 2018.
- 589 Rignot, E., Mouginit, J., Scheuchl, B., van den Broeke, M., van Wessem, M. J., & Morlighem, M.  
590 ~~(2019, January 22)~~: Four decades of Antarctic ice sheet mass balance from 1979–2017.  
591 *Proceedings of the National Academy of Sciences of the United States of America*. National  
592 Academy of Sciences. <https://doi.org/10.1073/pnas.1812883116>, 2019.

- 593 Rintoul, S. R., Silvano, A., Pena-Molino, B., van Wijk, E., Rosenberg, M., Greenbaum, J. S., &  
594 Blankenship, D. D.: ~~(2016)~~. Ocean heat drives rapid basal melt of the Totten ice shelf. *Science*  
595 *Advances*, 2(12). <https://doi.org/10.1126/sciadv.1601610>, 2016.
- 596 Scambos, T., Fahnestock, M., Moon, T., Gardner, A., & Klinger, M.: ~~(2016)~~. Global Land Ice  
597 Velocity Extraction from Landsat 8 (GoLIVE). Boulder, Colorado USA. NSIDC: National  
598 Snow and Ice Data Center, 2016.:-
- 599 Scambos, T. A., Haran, T. M., Fahnestock, M. A., Painter, T. H., & Bohlander, J.: ~~(2007)~~. MODIS-  
600 based Mosaic of Antarctica (MOA) data sets: Continent-wide surface morphology and snow  
601 grain size. *Remote Sensing of Environment*, 111(2), 242–257.  
602 <https://doi.org/10.1016/J.RSE.2006.12.020>, 2007.
- 603 Scherler, D., Leprince, S., & Strecker, M. R.: ~~(2008)~~. Glacier-surface velocities in alpine terrain  
604 from optical satellite imagery—Accuracy improvement and quality assessment. *Remote*  
605 *Sensing of Environment*, 112(10), 3806–3819. <https://doi.org/10.1016/J.RSE.2008.05.018>,  
606 2008.
- 607 Schröder, L., Horwath, M., Dietrich, R., & Helm, V.: ~~(2019)~~. Four decades of surface elevation  
608 change of the Antarctic Ice Sheet from multi-mission satellite altimetry. *The Cryosphere*, 13,  
609 427–449, <https://doi.org/10.5194/tc-13-427-2019>, 2019.
- 610 Smith, B., Fricker, H. A., Gardner, A. S., Medley, B., Nilsson, J., Paolo, F. S., Nicholas Holschuh,  
611 et al.: ~~(2020)~~. Pervasive ice sheet mass loss reflects competing ocean and atmosphere  
612 processes. *Science*, 368(6496), 1239–1242, 2020.:-
- 613 Sproson, A. D., Takano, Y., Miyairi, Y., Aze, T., Matsuzaki, H., Ohkouchi, N., & Yokoyama, Y.:  
614 ~~(2021)~~. Beryllium isotopes in sediments from Lake Maruwan Oike and Lake Skallen, East  
615 Antarctica, reveal substantial glacial discharge during the late Holocene. *Quaternary Science*  
616 *Reviews*, 256, 106841. <https://doi.org/10.1016/J.QUASCIREV.2021.106841>, 2021.
- 617 Stokes, C.R., Abram, N.J., Bentley, M.J. et al.: Response of the East Antarctic Ice Sheet to past and  
618 future climate change. *Nature* 608, 275–286 ~~(2022)~~.- [https://doi.org/10.1038/s41586-022-](https://doi.org/10.1038/s41586-022-04946-0)  
619 [04946-0](https://doi.org/10.1038/s41586-022-04946-0), 2022
- 620 Thoma, M., Jenkins, A., Holland, D., & Jacobs, S.: ~~(2008)~~. Modelling Circumpolar Deep Water  
621 intrusions on the Amundsen Sea continental shelf, Antarctica. *Geophysical Research Letters*,  
622 35(18). <https://doi.org/10.1029/2008GL034939>, 2008.
- 623 Thompson, D. W. J., & Solomon, S.: ~~(2002)~~. Interpretation of recent Southern Hemisphere climate  
624 change. *Science*, 296(5569), 895–899. <https://doi.org/10.1126/science.1069270>, 2002.
- 625 Thompson, D. W. J., Solomon, S., Kushner, P. J., England, M. H., Grise, K. M., & Karoly, D. J.:  
626 ~~(2011)~~. Signatures of the Antarctic ozone hole in Southern Hemisphere surface climate change.  
627 *Nature Geoscience* 2011 4:11, 4(11), 741–749. <https://doi.org/10.1038/ngeo1296>, 2011.
- 628 Toh, H. and Shibuya, K.: ~~(1992)~~. Thinning rate of ice sheet on Mizuho Plateau, East Antarctica,  
629 determined by GPS differential positioning. In Yoshida, Y., Kaminuma, K. and Shiraiishi, K.,  
630 eds. Recent progress in Antarctic earth sciences. Tokyo, Terra Scientific Publishing Co., 579–  
631 583, 1992.:-
- 632 Turner, J., Colwell, S. R., Marshall, G. J., Lachlan-Cope, T. A., Carleton, A. M., Jones, P. D.,  
633 Lagun, V., Reid, P. A., & Iagovkina, S.: ~~(2004)~~. The SCAR READER Project: Toward a High-

- 634 Quality Database of Mean Antarctic Meteorological Observations, *Journal of Climate*, 17(14),  
635 2890-2898, 2004.
- 636 Turner, J.: ~~(2005)~~. Antarctic climate change during the last 50 years. *Int. J. Climatol.*, 25, 279–294,  
637 2005.
- 638 Wang, G., Cai, W., & Purich, A.: ~~(2014)~~. Trends in Southern Hemisphere wind-driven circulation  
639 in CMIP5 models over the 21st century: Ozone recovery versus greenhouse forcing. *Journal of*  
640 *Geophysical Research: Oceans*, 119(5), 2974–2986. <https://doi.org/10.1002/2013JC009589>,  
641 2014.
- 642 Yin, J. H.: ~~(2005)~~. A consistent poleward shift of the storm tracks in simulations of 21st century  
643 climate. *Geophys. Res. Lett.*, 32(18), L18701. <https://doi.org/10.1029/2005gl023684>, 2005.
- 644